Polymer 50 (2009) 5851–5864

Contents lists available at ScienceDirect

Polymer

journal homepage: www.elsevier.com/locate/polymer

A comprehensive model for kinetics and development of film structure in interfacial polycondensation

Sunil S. Dhumal, A.K. Suresh*

Department of Chemical Engineering, Indian Institute of Technology Bombay, Mumbai 400076, India

ARTICLE INFO

Article history:
Received 20 August 2009
Received in revised form
26 September 2009
Accepted 28 September 2009
Available online 2 October 2009

Keywords:
Interfacial polycondensation
Modeling of film formation
Molecular weight distribution

ABSTRACT

A detailed model for interfacial polycondensation (IP) reaction, which accounts for the salient equilibrium and rate processes in reaction and phase separation, is reported here. The modeling of nucleation phenomena is more rational and fundamentally based than so far attempted in the literature on this process. Simpler models are proposed for situations in which one of transport and reaction resistances is the dominant one, and criteria developed that guide the selection of the model. The model explains the empirical findings on different interfacial systems, which have been reported in the literature. An extensive parametric study has been carried out in order to explain the effect of the important dimensionless parameters that arise, and analysis shows that most of the effects observed can be rationalized with respect to certain types of asymptotic behavior. The model makes it possible to predict the time course of development of the important film properties such as thickness, MWD and crystallinity, and to relate these to the preparation conditions and system parameters, as embodied in the different dimensionless parameters. It should therefore be possible to use this model to choose synthesis conditions and system-dependent parameters to achieve desired properties.

1. Introduction

Interfacial polycondensation (IP) is a step growth polymerization technique in which two monomers dissolved in mutually immiscible phases react at the phase-interface, with the polymer product forming a film separating the two phases. The technique has been studied in the context of applications ranging from bulk polymer synthesis (notably polycarbonates [1,2], but also for other polymers difficult to synthesize by melt methods [3]), to such niche applications such as micro/nano-encapsulation [4–8], thin film composite/nanocomposite membranes (TFCM) [9–15] and polymer nanocomposites [16,17]. It has also attracted attention in the context of surface modification of fibers [18,19], micro-unit operations [20,21] and self-healing materials [22]. The inherent heterogeneity of the process, the interplay of physical and chemical kinetics, and the role of polymer solution thermodynamics and phase separation render the overall reaction mechanism sufficiently complex, that a detailed understanding of how preparation conditions influence kinetics and film structure is rendered difficult [23].

Interest in IP goes back several decades, and early experimental work on the fundamental features [3,24–26] provided a basis for subsequent attempts at mathematical modeling of the process [23,27–29]. The manner in which the reaction locale and the mechanism of film formation are conceptualized, forms a basis on which the modeling approaches may be classified. The mechanism of phase separation has been shown to be important in determining microstructure and film properties in other situations, such as membrane casting from solution [30], and hence with IP too, we may expect incorporation of these aspects into models to be of central importance, if such models are to predict polymer properties with any degree of fidelity. Properties such as crystallinity, molecular weight distribution (MWD), and morphology of the film have a strong bearing on the functional suitability of the polymer or structures produced by the technique, and their evolution as well as their dependence on preparation conditions, are likely to be significantly influenced by the mechanism of phase separation. As Berzkin and Khokhlov [29] note after a study of the literature, the need for systematic and detailed theoretical and experimental studies continues to remain high in order to converge on a fundamental understanding of the process and the importance of preparation and physicochemical parameters on kinetics and film structure. This need motivates the present study, which is part of an ongoing program on IP in which results of experiments are used to develop improved models and the model predictions are used to plan newer experiments.

Dhumal et al. [23] have recently reviewed the literature on the modeling studies on IP. They recognize three basic approaches in treating phase separation and film formation. In the first, the

* Corresponding author. Tel.: +91 22 25767240; fax: +91 22 25726895.
E-mail address: aksuresh@iitb.ac.in (A.K. Suresh).

0032-3861/$ – see front matter © 2009 Elsevier Ltd. All rights reserved.
doi:10.1016/j.polymer.2009.09.072

Nomenclature

a_{if}	Interfacial area, m^2
a_I	Interfacial area per unit volume of aqueous phase, m^{-1}
A_{mr}	A type oligomer concentration in the reaction zone of chain length m, kmol/m^3
A_{0a}	Unprotonated concentration of A type monomer in bulk aqueous phase, kmol/m^3
A_{0ap}	A type monomer concentration at the aqueous phase-polymer interface, kmol/m^3
A_{0r}	A type monomer concentration in the reaction zone, kmol/m^3
A_T	Total concentration of A type monomer in the bulk aqueous phase, kmol/m^3
A_{T0}	Initial total concentration of A type monomer in the bulk aqueous phase, kmol/m^3
B_{mr}	B type oligomer concentration in the reaction zone of chain length m, kmol/m^3
B_{0r}	B type monomer concentration in the reaction zone, kmol/m^3
B_{0s}	B type monomer concentration in the bulk organic phase, kmol/m^3
B_{0s}^0	Initial B type monomer concentration in the bulk organic phase, kmol/m^3
C_{mr}	C type oligomer concentration in the reaction zone of chain length m, kmol/m^3
d_p	Diameter of microcapsule, m
D_{A0}	Diffusion coefficient of A type monomer through the polymer film, m^2/s
h	Hydrogen ion concentration
k	Reaction rate constant between $-A$ and $-B$, m^3/kmol s
k'_m	Nucleation rate constant, #/m^3 s
k_{LA0}	External mass transfer coefficient in the aqueous film, m/s
k_{LB0}	External mass transfer coefficient in the organic film, m/s
$K_{A_{0ap}}$	Partition coefficient of A type monomer between aqueous phase and polymer film
$K_{A_{0sa}}$	Partition coefficient of A type monomer between solvent and aqueous phase
$K_{A_{0sp}}$	Partition coefficient of A type monomer between polymer film and solvent
M_A	Molecular weight of A-monomer, kg/kmol
M_B	Molecular weight of B-monomer, kg/kmol
$M_{Y_{mr}}$	Molecular weight of Y_{mr} species, kg/kmol
n_{max}	Maximum number of oligomeric species
n_L	Number of moles of limiting monomer, kmol
N_{CN}	Number of critical nuclei, #/m^3
$r_{Y_{mr}}$	Rate of generation of Y_{mr} species, kmol/m^3 s
$r_{Y_{mr}ppt}$	Rate of precipitation of Y_{mr} species, kmol/m^3 s
R	Mole ratio of B type to A type monomer in bulk
R_{CN}	Critical nuclei radius, m
t	Time, sec
V_a	Volume of aqueous phase, m^3
V_s, V_d	Volume of dispersed organic phase, m^3
X	Fractional conversion of A type of monomer
X_B	Fractional conversion of B type of monomer
Y_{mr}	Concentration of oligomeric species of chain length m, kmol/m^3

Greek letters

α_s	Swelling index
ε	Reaction zone thickness, m
δ_m	Maximum polymer film thickness, m
δ_t	Polymer film thickness at time t, m
Φ	Volume fraction
τ	Non-dimensional time
σ	Interfacial energy between nucleus and surrounding lean phase, J/m^2
ρ_{Y_m}	Density of Y_{mr} species, kg/m^3
ρ_p	Density of polymer, kg/m^3

Superscripts

*	Non-dimensional quantity
$'bn$	Binodal, polymer lean phase
$''bn$	Binodal, polymer-rich phase
$'sp$	Spinodal, polymer lean phase

Subscripts

n,m	Oligomer species number
r	Reaction zone
s	Organic solvent
t	Total
Y_{mr}	Type of species either A_{mr}, B_{mr} or C_{mr}

solubility of polymer is taken to be negligible, and the entire polymer formed goes to form the film. In the second, the polymer, which forms in a thin reaction zone on the organic side of the interface, forms a separate phase (with further heuristics determining the conditions under which the phase-separated material coalesces to a film) as the concentration increases beyond a solubility limit, calculated from considerations of polymer solution thermodynamics. In the third, film formation is visualized as a gradual thickening/gelification of the reaction zone itself. The second approach is sufficiently comprehensive and allows for consideration of different mechanisms of phase separation such as nucleation and spinodal decomposition. With this approach, Dhumal et al. [23] were able to predict the MWD, crystallinity and thickness of the film. While some qualitative success was achieved in predicting certain trends, the work highlighted the need for better description of the phase separation mechanisms, as well as the need for specific types of data to validate the model precepts.

A second aspect, which has been often mentioned [27,31] in connection with parameter estimation is the issue of controlling regimes in IP, since several transport and reaction steps are involved. While criteria have been developed to recognize the controlling regime and hence to strategize parameter estimation, how differences in preparation conditions translate to differences in polymer and film properties under various controlling regimes has so far not been examined under any model.

The present work is inspired by the above gaps in the literature. In this paper, we develop a model based on the concept of a reaction locale of finite thickness, in which the phenomena of multi-step polymerization reaction, nucleation and spinodal decomposition all occur. Since critical nucleus sizes predicted by classical nucleation theory increase rapidly at compositions close to the binodal limit, nucleation rate has to decrease sufficiently rapidly with supersaturation so that the possibility of formation of unreasonably large nuclei is avoided. We employ a formulation of nucleation kinetics that achieves this, and hence eliminates the need for artificial constraints on the size of the nucleus that can form, as was required in earlier efforts. The model has been simplified for the cases of diffusion and kinetic control, and the sub-models that result make it possible to study the distinguishing features of these regimes, not only in terms of kinetics, but also in

terms of product quality parameters, in detail. Extensive analysis coupled with parametric studies has been carried out to understand the features of the model. Aspects of the model have been justified based on information available in the literature.

2. Model development

The model developed here takes as its basis, the model of Dhumal et al. [23]. The following description assumes, for convenience and with the experimental system that has inspired the development of the model in mind, that the aqueous phase monomer (monomer *A*) is a diamine and the organic phase monomer (monomer *B*), a diisocyanate. The model is shown schematically in Fig. 1, considering a small section of the aqueous–organic interface with the formed polymer film separating the phases at some intermediate stage of the reaction. The un-ionized part of monomer *A* diffuses from the aqueous phase through the formed polymer film and reacts with monomer *B* in a thin reaction zone located on the organic side. The complete set of reactions includes the reactions among the oligomers, as well as of the monomers with the oligomers, and results in three types of oligomers of various chain lengths – amine-terminated (*A*), isocyanate-terminated (*B*), and amine-isocyanate-terminated (*C*), with general formulae as given in Table 1. The concentrations of the oligomers in solution are determined by a balance between the rates of reactions that form and consume them, and phase separation. The latter, for each oligomer, is in turn governed by the concentration of the oligomer in relation to the binodal and spinodal solubility limits, here calculated using the Flory–Huggins theory. Nucleation governs phase separation when the oligomer composition is in the metastable region, while spinodal decomposition governs when the composition reaches the spinodal limit. Phase-separated oligomers do not take any further part in reactions. Other details are as described in Dhumal et al. [23].

The phase separation mechanisms play an important role in the model, since they not only control the concentration of the oligomers (and hence the molecular weight distribution), but also the crystallinity of the phase-separated polymer. In the previous work, the critical nucleus size was calculated using the classical nucleation theory, but a phenomenological rate expression, earlier used by Gonzalez-Ortiz and Asua [32] was used to express the rate of phase separation by nucleation. This assumes the volumetric rate of nucleation as being linear in the supersaturation with respect to the binodal limit (reckoned in volume fraction terms). One would expect that at low levels of supersaturation, since the predicted nucleus size is very large, the probability of formation of such a nucleus would be very small. The rate expression does not quite

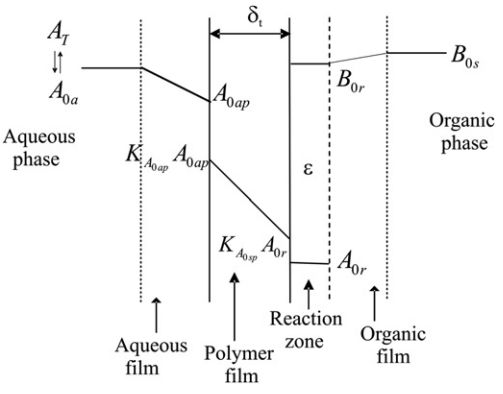

Fig. 1. Schematic showing the concentration profiles across the polymer film during IP reaction.

Table 1
General formulae for the different oligomeric and monomeric species that form during the reaction. The polyurea system is taken as the example here (A–: NH_2–: B–:NCO–;R:$(CH_2)_6$; R′: $(CH_2)_6$).

Notation	Species	Structure
–*X*–	Repeat Unit	–[*NH–OCNH–R′–NHCO–NH–R*]–
A_0	HMDA	*A–R–A*
B_0	HMDI	*B–R′–B*
C_0	Oligomer	*A–R–NH–NHCO–R′–B*
A_n	Oligomer	$A–R–X_n–A$
B_n	Oligomer	$B–R'–X_n–B$
C_n	Oligomer	$A–R–X_n–NH–NHCO–R'–B$

account for this, with the result that an artificial limit had to be imposed on the maximum size of the nucleus that could be formed. In the present work, we use the formalism proposed by Kamide et al. [33] based on classical nucleation theory consistently, which eliminates the need to impose such limits.

2.1. Nucleation kinetics

According to the classical nucleation theory, as the volume fraction nears the binodal limit, one would expect a rapid decrease in the nucleation rate. This is because of a rapid increase in the free energy barrier to nucleation as the supersaturation with respect to the binodal limit approaches zero. Following Kamide et al. [33], we express the rate of formation of critical nuclei of oligomer of chain length *m*, Y_{mr} (where *Y* stands for *A*, *B* or *C* according as the oligomer is amine, isocyanate, or amine-isocyanate ended), as

$$\frac{dN_{CNY_{mr}}}{dt} = \left\{k'_m \exp\left(-\frac{\Delta\phi_{CNY_{mr}}}{k_B T}\right)\right\}\left(1 - \frac{N_{CNY_{mr}}(t)}{N_{CNY_{mr}}(\infty)}\right)$$
$$m = 1 \text{ to } n_{max} \quad \text{for } Y_{mr} = A_{mr} \text{ and } B_{mr}$$
$$m = 0 \text{ to } n_{max} \quad \text{for } Y_{mr} = C_{mr} \tag{1}$$

where, $N_{CNY_{mr}}$ is the number of critical nuclei per unit volume (of the polymer-rich phase), of the oligomer Y_{mr}. The first term on the right (within braces) can be regarded as a nucleation rate constant, with an Arrhenius' type dependence on temperature. The activation energy barrier $\Delta\phi_{CNY_{mr}}$ increases rapidly as the composition gets close to the binodal limit, being given by:

$$\Delta\phi_{CNY_{mr}} = \frac{16\pi\sigma^3_{Y_{mr}}}{3\Delta f^2_{\nu Y_{mr}}} \tag{2}$$

where, $\sigma_{Y_{mr}}$ is interfacial energy and $\Delta f_{\nu Y_{mr}}$ is the Gibbs free energy change corresponding to the formation of the critical nucleus of species Y_{mr}. Expressions for $R_{CNY_{mr}}$, $\sigma_{Y_{mr}}$ and $\Delta f_{\nu Y_{mr}}$ are the same as used in earlier work [23].

The driving force for nucleation, in equation (1), is seen to be the fractional difference between the actual number of nuclei and the maximum number possible at the prevailing level of supersaturation, $N_{CNY_{mr}}(\infty)$. The latter can be taken as the number that can form if all supersaturation were to be discharged (as nuclei of the polymer-rich phase) with the prevailing size of the critical nucleus:

$$N_{CNY_{mr}}(\infty) = \frac{3\left(\Phi_{Y_{mr}} - \Phi'^{bn}_{Y_{mr}}\right)}{4\pi R^3_{CNY_{mr}}\left(\Phi''^{bn}_{Y_{mr}} - \Phi'^{bn}_{Y_{mr}}\right)} \tag{3}$$

As we consider the effect of supersaturation (i.e., distance from binodal) on nucleation kinetics, we see that in the present formulation, the rate decreases as the supersaturation tends to zero, due to two reasons – decrease in the driving force term itself, as well as an increase in the activation energy barrier. Nucleation rates, as conceptualized in this and previous work [23] are compared in Fig. 2, in which is plotted the volumetric nucleation rate

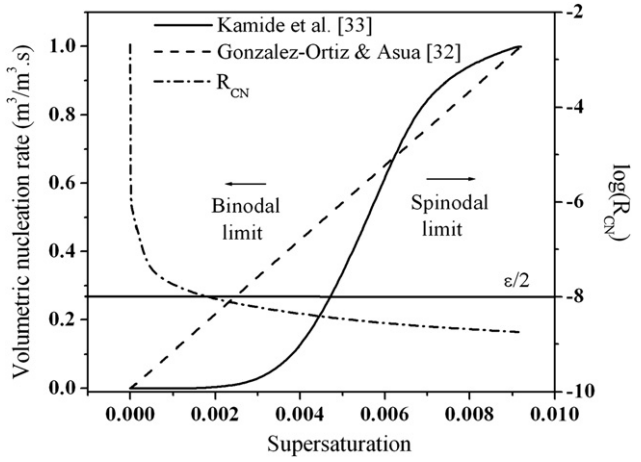

Fig. 2. Comparison of nucleation rates as given by different expressions.

(normalized with respect to the rate just under the spinodal limit), as a function of supersaturation in the metastable region. Volumetric nucleation rates have been calculated in the present case by multiplying the number rate of nucleation (equation (1)) by the volume of a single nucleus (the assumption being that R_{CN} is a relatively weak function of supersaturation, which holds true except at very small supersaturations). These calculations refer to a typical oligomer in the polyurea system (B_5), and a temperature of 30 °C. Also shown for comparison is the variation in R_{CN}. It is seen that, contrary to the earlier model, the present formulation correctly has the volumetric nucleation rate rapidly declining to zero in spite of an increase in R_{CN}. In particular, under conditions at which the nucleus size is comparable to the thickness of the reaction zone, the earlier model would still predict finite rates of nucleation, a fact that made it necessary, in earlier work, to set the nucleation rate as zero for such large nuclei. In the present case, it is seen that the nucleation rate naturally goes to zero, so that such arbitrary limits are not needed.

2.2. Species mass balances and auxiliary equations

The mole balance equations for the various monomer and oligomeric species are written in a manner similar to Dhumal et al. [23], except for the above difference in the manner in which nucleation rate is treated. We non-dimensionalize the equations by defining dimensionless variables, which are given in Table 2.

The model equations in terms of these dimensionless variables are given below:

$$\frac{dX}{d\tau} = \frac{1}{\left[1+\delta^*/F_1\right]}\left(\frac{1-X}{f\left(h^*\right)} - RF_2K_{A0sa}A^*_{0r}\right) \tag{4}$$

$$\frac{dX_B}{d\tau} = F_2\left(1-X_B-B^*_{0r}\right) \tag{5}$$

$$\frac{dA^*_{0r}}{d\tau} = \frac{1}{F_3\left[1+\delta^*/F_1\right]}\left(\frac{1-X}{RF_2f\left(h^*\right)} - K_{A0sa}A^*_{0r}\right) - F_4A^*_{0r}\left[S^*_B+0.5S^*_C\right] \tag{6}$$

$$\frac{dB^*_{0r}}{d\tau} = \frac{1}{F_3}\left(1-X_B-B^*_{0r}\right) - F_4B^*_{0r}\left[S^*_A+0.5S^*_C\right] \tag{7}$$

Table 2
Definitions of dimensionless variables used in the model equations (n_{max} is the maximum chain length assumed for the purpose of computations; $N_{CNY_{mr}\inf} = N_{CNY_{mr}}(\infty)$ when $\Phi_{Y_{mr}} = \Phi^{sp}_{Y_{mr}}$; see equation (3)).

Quantity	Symbol	Definition	Number of variables
Aqueous phase monomer conversion	X	$1-(A_T/A_{T0})$	1
Organic phase monomer conversion	X_B	$1-(B_{0s}/B^0_{0s})$	1
Hydrogen ion concentration	h^*	h/K_{a2}	1
Concentration of oligomer	Y^*_{mr}	Y_{mr}/B^0_{0s}	$3n_{max}+1$
Radius of critical nucleus of species Y_{mr}	$R^*_{CNY_{mr}}$	$R_{CNY_{mr}}/\varepsilon$	$3n_{max}+1$
Number of critical nuclei of species Y_{mr}	$N^*_{CNY_{mr}}$	$N_{CNY_{mr}}/N_{CNY_{mr}\inf}$	$3n_{max}+1$
Max. number of critical nuclei of species Y_{mr} at the prevailing supersaturation	$N^*_{CNY_{mr}}(\infty)$	$N_{CNY_{mr}}(\infty)/N_{CNY_{mr}\inf}$	$3n_{max}+1$
Film thickness	δ^*	δ_t/δ_m	1
Activation energy barrier for nucleation of species Y_{mr}	$\Delta\phi_{CNY_{mr}}/k_b$	$\frac{16\pi\sigma^3_{Y_{mr}}}{3k_BTJf^2_{vY_{mr}}}$	$3n_{max}+1$
Time of reaction	τ	$a_lk_{LA0}t$	1

$$\frac{dA^*_{mr}}{d\tau} = F_4\left(0.5\sum_{n=0}^{m-1}A^*_{(m-n-1)r}C^*_{nr} - A^*_{mr}\left(S^*_B+0.5S^*_C\right)\right) - \frac{F_5F_{6A_{mr}}}{\mathbb{N}_{min}}\frac{4\pi R^{*3}_{CNA_{mr}}}{3}\exp\left(-\frac{\Delta\phi_{CNA_{mr}}}{k_BT}\right)\left(1-\frac{N^*_{CNA_{mr}}(\tau)}{N^*_{CNA_{mr}}(\infty)}\right) u\left(\Delta A^{*\prime bn}_{mr}\right) \quad m = 1 \text{ to } n_{max} \tag{8}$$

$$\frac{dB^*_{mr}}{d\tau} = F_4\left(0.5\sum_{n=0}^{m-1}B^*_{(m-n-1)r}C^*_{nr} - B^*_{mr}\left(S^*_A+0.5S^*_C\right)\right) - \frac{F_5F_{6B_{mr}}}{\mathbb{N}_{min}}\frac{4\pi R^{*3}_{CNB_{mr}}}{3}\exp\left(-\frac{\Delta\phi_{CNB_{mr}}}{k_BT}\right)\left(1-\frac{N^*_{CNB_{mr}}(\tau)}{N^*_{CNB_{mr}}(\infty)}\right) u\left(\Delta B^{*\prime bn}_{mr}\right) \quad m = 1 \text{ to } n_{max} \tag{9}$$

$$\frac{dC^*_{mr}}{d\tau} = F_4\left(\sum_{n=0}^{m}A^*_{(m-n)r}B^*_{nr} + 0.5\sum_{n=0}^{m-1}C^*_{(m-n-1)r}C^*_{nr} - 0.5C^*_{mr}\left(S^*_A+S^*_B+S^*_C\right)\right) - \frac{F_5F_{6C_{mr}}}{\mathbb{N}_{min}}\frac{4\pi R^{*3}_{CNC_{mr}}}{3}\exp\left(-\frac{\Delta\phi_{CNC_{mr}}}{k_BT}\right)\left(1-\frac{N^*_{CNC_{mr}}(\tau)}{N^*_{CNC_{mr}}(\infty)}\right)u\left(\Delta C^{*\prime bn}_{mr}\right) \quad m = 0 \text{ to } n_{max} \tag{10}$$

$$\frac{dN^*_{CNY_{mr}}}{d\tau} = \frac{F_5}{\mathbb{N}_{max\mathbb{Y}_{mr}}}\exp\left(-\frac{\Delta\phi_{CNY_{mr}}}{k_BT}\right)\left(1-\frac{N^*_{CNY_{mr}}(\tau)}{N^*_{CNY_{mr}}(\infty)}\right) \quad m = 1 \text{ to } n_{max} \quad \text{for } Y_{mr} = A_{mr} \text{ and } B_{mr}, \quad m = 0 \text{ to } n_{max} \quad \text{for } Y_{mr} = C_{mr} \tag{11}$$

$$X = 1-\left(\frac{h^*}{h^*_0}\right)^{-p} \tag{12}$$

$$R^*_{CNY_{mr}} = -\frac{2\sigma_{Y_{mr}}}{\varepsilon\Delta f_{vY_{mr}}} \tag{13}$$

$$\delta^* = \frac{\delta_t}{\delta_m} = \frac{6\delta_t \rho_p V_d}{M_{C0} d_p \alpha_s n_L} \tag{14}$$

In the above equations,

$$S_A^* = \sum_{n=0}^{n_{\max}} A_{nr}^*;\ S_B^* = \sum_{n=0}^{n_{\max}} B_{nr}^*;\ S_C^* = \sum_{n=0}^{n_{\max}} C_{nr}^*;$$

$$f\left(h^*\right) = \left(1 + h^* + h^{*2} K_{a2}/K_{a1}\right)$$

The dimensionless hydrogen ion concentration h^* enters into the equations in the general case in which the monomer consumption leads to a fall in pH, which in turn influences the availability of monomer A (since only the unprotonated form can participate in the reaction). pH is related to the monomer concentration and a calibration function is usually used to express one in terms of the other [34], which leads to equation (12).

In equation (14), the actual film thickness (δ_t) is calculated as the sum of two contributions – one (δ_{tX}) from nucleated material and the other (δ_{tNX}), from spinodal decomposition as discussed in the previous study [23]. While nuclei form at a rate given by equation (11) as discussed above, these nuclei are assumed to coalesce and form a film when the projected area of all the nuclei equals the available area. Spinodal decomposition occurs at any time during the reaction, if the composition hits the spinodal limit, and at such an event, any existing nuclei are also swept into the incremental film that forms.

The dimensionless groups occurring in the above equations are:

$$F_1 = \frac{D_{A0} K_{A0ap}}{k_{LA0} \delta_m};\ F_2 = \frac{V_a}{V_s - V_r} \approx \frac{V_a}{V_d};\ F_3 = a_I \varepsilon;\ F_4 = \frac{B_{0s}^0 k_i}{k_{LA0} a_I};$$

$$F_5 = \frac{k_m' V_r}{k_{LA0} a_I};\ F_{6Y_{mr}} = \frac{\rho_{Y_m} \Phi_{Y_{mr}}'^{bn}}{B_{0s}^0 M_{Y_m}};$$

$$N_{\min} = V_r/\varepsilon^3;\ N_{\max Y_{mr}} = N_{CNY_{mr}\inf} V_r$$

F_1, F_4 and F_5 compare respectively the characteristic times of diffusion, reaction and nucleation to that of external mass transfer. F_2 and F_3 are volume ratios (aqueous-to-organic and reaction zone-to-aqueous). $F_{6Y_{mr}}$ are dimensionless upper binodal limits, one for each oligomeric species. $N_{\max Y_{mr}}$ and $N_{\min}$ are the maximum and minimum possible numbers of critical nuclei with smallest and biggest size, respectively.

While, for the sake of generality, the characteristic time of mass transfer has been used above to non-dimensionalize the time, external mass transfer resistance is not significant for a number of applications of interest [27]. For such cases therefore, the following groups, which express the relative rates of the relevant rate processes are more appropriate in parametric studies:

$$F_{14} = F_4/F_1 = \frac{\text{Diffusion time}}{\text{Reaction time}} = \frac{\delta_m B_{0s}^0 k_i}{D_{A0} K_{A0ap} a_I} \tag{15}$$

$$F_{15} = F_5/F_1 = \frac{\text{Diffusion time}}{\text{Nucleation time}} = \frac{k_m' \delta_m V_r}{D_{A0} K_{A0ap} a_I} \tag{16}$$

$$F_{45} = F_5/F_4 = \frac{\text{Reaction time}}{\text{Nucleation time}} = \frac{k_m' V_r}{B_{0s}^0 k_i} \tag{17}$$

For experimental studies in microencapsulation, Wagh et al. [34] found it convenient to work in terms of a set of 'experimental variables', namely, n_L/V_d, R and V_d/V_a. These variables determine the values of the dimensionless groups defined above for a system with a known mean drop size (d_p), mass transfer coefficient (k_{LA0}) and monomer chemistry:

$$F_1 = \frac{6 D_{A0} K_{A0ap} \rho_p}{k_{LA0} M_{C_{0r}} d_p \alpha_s} \left(\frac{V_d}{n_L}\right) \tag{18}$$

$$F_3 = \frac{6\varepsilon}{d_p}\left(\frac{V_d}{V_a}\right) = \frac{6\varepsilon}{F_2 d_p} \tag{19}$$

$$\begin{aligned} F_4 &= \frac{k_i d_p}{6 k_{LA0}} \left(\frac{R(n_L/V_d)}{(V_d/V_a)}\right) \quad \text{if } R > 1 \\ &= \frac{k_i d_p}{6 k_{LA0}} \left(\frac{(n_L/V_d)}{(V_d/V_a)}\right) \quad \text{if } R < 1 \end{aligned} \tag{20}$$

$$F_5 = \frac{k_m' a_{if} \varepsilon}{k_{LA0} a_{if}/V_a} = \frac{k_m' \varepsilon V_a}{k_{LA0}} \tag{21}$$

The differential equations (4)–(11) form a set of $6n_{\max}+6$ equations to be solved simultaneously with the other algebraic relationships. The initial conditions that apply are:

$$\tau = 0;\ B_{0s}^{0*} = B_{0r}^* = 1;\ X = X_B = A_{0r}^* = Y_{mr}^* = N_{\mathrm{CNY}_{mr}}^* = 0$$

The solutions are used to calculate polymer properties such as the crystallinity, molecular weight distribution and polydispersity at any reaction time. Crystallinity is calculated by assuming the nucleated material to be of maximum crystallinity (as allowed by the structure [35]) and spinodally decomposed material to be completely amorphous. Further details of property calculation are available in Dhumal et al. [23].

2.3. Simplified models for situations in which a single resistance dominates

Three different resistances, external mass transfer, diffusion through polymer film and polycondensation reaction, have been considered in the above model. As remarked earlier, it is usually the latter two resistances that are more important, external mass transfer being quite fast. We may therefore examine scenarios in which one or the other of the two important resistances dominates to the extent of being a controlling resistance. Below, we cast the equations in a manner that facilitates the simplification of the general model to these special cases.

The overall driving force for the process may be regarded as the concentration of the unprotonated form of the aqueous phase monomer. This can be expressed as the sum of two parts, one of which drives the transport process and the other, the reaction process in series with it:

$$\frac{(1-X)}{f\left(h^*\right)} = \left[\frac{(1-X)}{f\left(h^*\right)} - RF_2 K_{A_{0sa}} A_{0r}^*\right] + RF_2 K_{A_{0sa}} A_{0r}^* \tag{22}$$

We may assume the monomer A to be at a quasi-steady state in the reaction zone. Equating the rates of transport and reaction of A in the reaction zone in equation (6) therefore,

$$\begin{aligned} \frac{\mathrm{d}X}{\mathrm{d}\tau} &= \frac{1}{\left[1 + \delta^*/F_1\right]} \left(\frac{1-X}{f\left(h^*\right)} - RF_2 K_{A0sa} A_{0r}^*\right) \\ &= F_4 F_3 RF_2 A_{0r}^* \left[S_B^* + 0.5 S_C^*\right] \end{aligned} \tag{23}$$

Substituting into equation (22), the rate of reaction can be written in the traditional resistance-driving force formulation as:

$$\frac{dX}{d\tau} = \frac{\text{Overall driving force}}{\text{Total resistance}} = \frac{(1-X)/f\left(h^*\right)}{\left(\left[1+\delta^*/F_1\right] + K_{A0sa}/\left(F_4F_3\left[S_B^* + 0.5S_C^*\right]\right)\right)} \quad (24)$$

Kinetic control

Under kinetic control, the transport resistance is negligible as compared to the kinetic resistance. So this situation is described in mathematical form as

$$\frac{dX}{d\tau} = F_4F_3\frac{(1-X)}{f\left(h^*\right)K_{A0sa}}\left[S_B^* + 0.5S_C^*\right] \quad (25)$$

Under these conditions, A_{0r}^* will achieve a value in equilibrium with the monomer concentration in the external phase: $A_{0r}^* = (1-X)/(RF_2K_{A_{0sa}}f(h^*))$. Thus, for a given system, the smaller the value of R, the larger the concentration of monomer A in the reaction zone.

Diffusion control

In the diffusion control regime, it is the term corresponding to the kinetic resistance in the denominator of equation (24) that can be neglected; the rate equation becomes:

$$\frac{dX}{d\tau} = \frac{1}{\left[1+\delta^*/F_1\right]}\frac{1-X}{f\left(h^*\right)} \quad (26)$$

Further, the concentration of the diffusing monomer will be zero in the reaction zone: $A_{0r}^* = 0$ (and so also will the concentration of other A-ended oligomeric species be zero).

The diffusing A is then divided among B and C type oligomers depending on their relative abundance in the reaction zone. For example, equation (10) for C_{0r}^* may be written as:

$$\frac{dC_{0r}^*}{d\tau} = \left(\frac{(1-X)}{RF_2F_3f\left(h^*\right)\left[1+\delta^*/F_1\right]}\right)\left(\frac{B_{0r}^*}{S_B^*+0.5S_C^*} - \frac{C_{0r}^*}{2S_B^*+S_C^*}\right) - 0.5F_4C_{0r}^*\left[S_B^*+S_C^*\right] - \frac{F_5F_{6C_{0r}}}{\mathbb{N}_{\min}}\frac{4\pi R_{CNC_{0r}}^{*3}}{3}\exp\left(-\frac{\Delta\phi_{CNC_{0r}}}{k_BT}\right)\left(1-\frac{N_{CNC_{0r}}^*(\tau)}{N_{CNC_{0r}}^*(\infty)}\right)u\left(\Delta C_{0r}^{*/bn}\right) \quad (27)$$

and similarly for other oligomer mole balances.

3. Results and discussion

The model equations are solved as described in the previous study [23]. Order of magnitude calculation of solute penetration depths as detailed in the previous studies [23,31,36] indicate reaction zone thicknesses of the order of 10^{-8} m. Preliminary computations, with different reaction zone thicknesses in this range, on the volume fraction of nuclei residing in any size range showed that nuclei of diameter more than 2×10^{-8} m do not contribute to the total population. The thickness of the reaction zone was thus chosen as 2×10^{-8} m in all computations. Further, the values of parameters that determine the phase envelopes are assumed for the polyurea system unless otherwise indicated. The values of parameters held constant in the discussion of results that follows are collected together in Table 3.

Table 3
Parameters held constant in model simulations.

Parameter	Value	Source
k_{LA0}, k_{LB0}	5×10^{-3} m/s	Calculated (Sh = 2)
K_{a1}	$10^{-9.83}$	Dean [37]
K_{a2}	$10^{-10.93}$	Dean [37]
K_{A0ap}	0.375	Yadav [38]
K_{A0sa} (Cyclohexane)	320	Wagh et al. [34]
K_{A0sa} (Toluene)	56	Wagh et al. [34]
n_{max}	100	–
V_a	110×10^{-6} m^3	–
X_{max}	0.5	Van Krevelen [35]
α_s	1.6	Yadav [38]

3.1. Effective stoichiometry of monomer consumption and maximum reaction extent

The parameter R indicates in a broad way the deviation of the recipe employed in any particular case from the ideal stoichiometric requirement of equal moles of both monomers ($R = 1$). The actual ratio in which the two monomers are consumed would however, vary from this ideal, depending on which type of oligomers predominate and what the average chain length is, of the oligomers being formed. We can analyze the possibilities under some assumptions as follows. Firstly, the nature of the IP process is such that a preponderance of B-ended oligomers would be expected under most circumstances; this has also been shown in earlier simulations [23]. Referring to Table 1, this type of species has an excess of monomer B as compared to A, the ratio being:

$$\frac{\text{moles of monomer } B}{\text{moles of monomer } A} = \frac{RX_B}{X} = \frac{n+1}{n} \quad (28)$$

a result which can be interpreted as defining the stoichiometric requirement of monomers if the conditions are such as to produce an average chain length of n. This implies that the maximum reaction extent possible is limited by monomer A or B according as their ratio in the recipe is greater than or less than$((n+1)/n)$, where the average chain length of the final film is to be used. Two limiting cases may be identified: one in which the chains are long enough that the above ratio tends to 1, and one in which they do not grow beyond B_1, in which case the ratio is 2. Table 4 summarizes the limiting values for the conversions of A and B, calculated on this basis.

In Fig. 3, we plot the maximum conversions obtained from model calculations for different values of the important dimensionless groups, in relation to the above theoretical limits. It should be noted that a straight line for X_{max} in the small-R region (and correspondingly, a rectangular hyperbola for X_{Bmax} in the high-R region) can be defined for any assumed value of n, in accordance with equation (28), and would lie between the limits shown.

We observe from the large R region ($R > 1$) in Fig. 3 in general, that as the excess of B in the recipe over the stoichiometric requirement increases, the curves move closer to the short chain limit, indicating that large values of R lead to low molecular weights. To achieve high molecular weights, an excess of the aqueous phase monomer is therefore to be preferred [3,39].

Table 4
Maximum conversion of monomers in limiting cases.

Limiting case	Conversion	$R \le 1$	$1 < R < 2$	$R \ge 2$
Long chain limit	X_{max}	R	1	1
	X_{Bmax}	1	$1/R$	$1/R$
Short chain limit	X_{max}	$R/2$	$R/2$	1
	X_{Bmax}	1	1	$2/R$

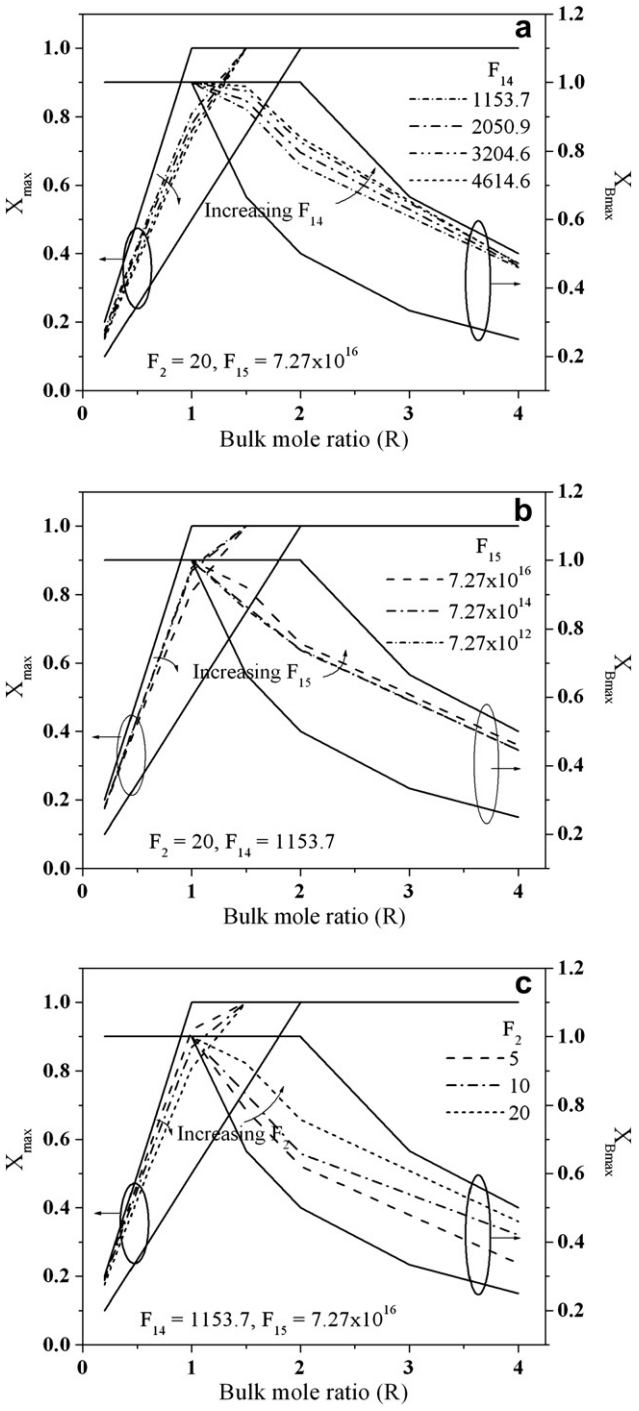

Fig. 3. Maximum conversions (X_{max} and X_{Bmax}) achieved as a function of R, for different values of (a) F_{14}, (b) F_{15} and (c) F_2 ($F_3 = 0.005$).

Fig. 3(a) shows that, for a given value of F_{15} and F_2, the larger the value of F_{14}, the closer is the overall stoichiometry to the short chain limit. F_{15} has a similar influence, as Fig. 3(b) show, for a constant F_{14} and F_2. Further, the effect of F_{15} is the more pronounced, the larger the value of F_{15}. Likewise, for constant F_{14} and F_{15}, the smaller the value of F_2, the closer the characteristic to the long chain limit as shown in Fig. 3(c). It is further observed that the effect of the parameters is in general more pronounced for cases of large R ($R > 1$). While the curves shown are for typical values of the parameters as noted in the figures, the trends are representative. These considerations help us to identify situations that lead to low molecular weights and those that lead to high molecular weights. Alternatively, measurements of molecular weights at different values of R can be used in conjunction with such plots for parameter estimation.

3.2. Reaction regimes

Every IP reaction starts off under kinetic control, but there is the likelihood of diffusion limitations once the film forms and starts growing. There are thus three possibilities- (i) the reaction proceeds under kinetic control over most of the conversion range, (ii) the reaction becomes diffusion controlled at a very small conversion and remains so over the rest of the conversion range, and (iii) the reaction switches from kinetic control to diffusion control over a range of conversions, so that the final film formed has comparable proportions formed under the dominance of either rate process. To know which of these possibilities applies in a particular case is important, since on this depends which parameter – k or D_{A0} – has an influence on the overall kinetics as well as film properties. In view of the complexity of the model and the number of different dimensionless groups that are involved in the model description, it is useful to attempt an approximate analysis to gain some insight into the important influences on reaction regime.

The importance of diffusion limitations on the process kinetics at any stage of reaction may be assessed by examining the dimensionless rate of reaction Ψ:

$$\Psi = \frac{A_{T0}(\mathrm{d}X/\mathrm{d}t)V_a}{(k_i B_{0s} A_T/f(h)K_{A_{0sa}})a_{if}\varepsilon} = \frac{(\mathrm{d}X/\mathrm{d}\tau)f\left(h^*\right)K_{A_{0sa}}}{F_3F_4(1-X_B)(1-X)} \tag{29}$$

which compares the actual rate with a characteristic rate in the absence of diffusion limitations (note how the characteristic rate is defined, based on the concentrations of B and un-ionized A in reaction zone). An insight into the effect of various parameters on Ψ can be obtained as follows. Since the concentration of the B-monomer in the reaction zone may be expected to be much higher than that of any other species, approximating $[S_B^* + S_C^*/2] \simeq B_{0r}^* \simeq B_{0s}^*$ in the quasi-steady state formulation (equation (24)), we may compare the resistances to diffusion transport of A and reaction through the quantity:

$$P = \frac{\text{transport resistance}}{\text{reaction resistance}} = \frac{\left[1+\delta^*/F_1\right]F_3F_4(1-X_B)}{K_{A0sa}} \approx \frac{F_{14}\delta^*(1-X_B)F_3}{K_{A0sa}} \tag{30}$$

The approximate form shown as the last term above is for the case of negligible external mass transfer resistance.

Fig. 4 shows the effect of P on Ψ on log-log co-ordinates, for different combinations of F_1, R and δ^* (the last in some sense showing the effect of reaction progress). The shape of the $\Psi - P$ curve is somewhat reminiscent of the effectiveness factor – Thiele modulus plot in diffusion-reaction situations [40], although in this case diffusion and reaction are in series and not simultaneous. Fig. 4 allows us to identify a region in the parameter space in which the process is kinetically controlled, and one in which the reaction is controlled by diffusion. Such regime identification helps in parameter estimation, as one can identify conditions under which a particular rate parameter influences the rate behavior to the exclusion of all others. It is seen that conditions of $P \ll 1$ lead to kinetic control while $P \gg 1$ leads to high levels of diffusion limitations.

The other fact that is clear from Fig. 4 is that the parameter P is successful in bringing together all the possible influences on regime

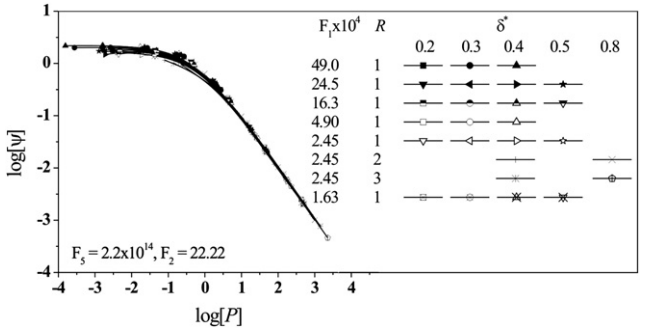

Fig. 4. Reaction regime plot showing the effect of the parameter P on the severity of diffusional limitations ($F_3 = 0.005$).

behavior, in large measure. The points for all combinations are seen to fall on a single curve, to a good approximation. Similar calculations for different values of F_5 and F_2 show that the curve shown in Fig. 4 applies in these cases also. Since F_5 is a dimensionless nucleation rate, it is clear that the phase separation mechanisms have no independent influence on the regime behavior (the range of values of F_5 chosen encompassed the entire spectrum from nucleation domination to spinodal decomposition-domination). It should be emphasized that for the system chosen (polyurea), the metastable region (of polymer volume fractions) is quite narrow, and the negligible influence of the nucleation rate constant is partly a reflection of this.

It is clear from the above that values of P for any system and at any stage of reaction may be used to assess the importance or otherwise of transport limitations. Calculation of the parameter P, from the estimated rate parameters of the previous experimental studies [38,41], shows that the microcapsule formation is, in general, a kinetically controlled process, in agreement with previous conclusions based on other criteria [23,27]. On the other hand, diffusion control is to be expected in the case of large droplets (i.e., small values of interfacial area per unit volume). The same conclusion can be extended to the unstirred film formation also i.e. during a typical unstirred film formation experiment a diffusion control would be expected. This is also in accordance with empirical evidence [3], which finds that the reaction almost stops once an initial film is formed.

As remarked earlier, Fig. 4 shows that a shift from kinetic control to diffusion control occurs when the parameter P goes above 1, i.e. when

$$\delta^*(1 - X_B) = K_{A0sa}/F_{14}F_3 \tag{31}$$

This equation defines, for a given set of system parameters, a value of conversion $X = X^*$(in so far as the left side is a function of X) at which the system passes from kinetic control to diffusion control. For those systems for which X^* is close to 1, kinetic control may be assumed to prevail over almost the entire course of reaction, and the simplified model for kinetic regime suffices. Similarly, for those systems for which X^* is close to zero, diffusion control may be assumed to prevail over almost the entire course of reaction, and the simplified diffusion regime model may be applied. It is only the remaining cases that call for an application of the detailed model. In view of the importance of this conclusion, it is worthwhile examining how the left side of equation (31) depends on X. The relationship between X and X_B depends on the overall stoichiometry of monomer consumption (equation (28)), which has been discussed earlier. Typical model simulation results for the relation between X_B and X are shown in Fig. 5 for different values of the important parameters with the short and long chain limiting cases plotted alongside for reference. While the influence of the different

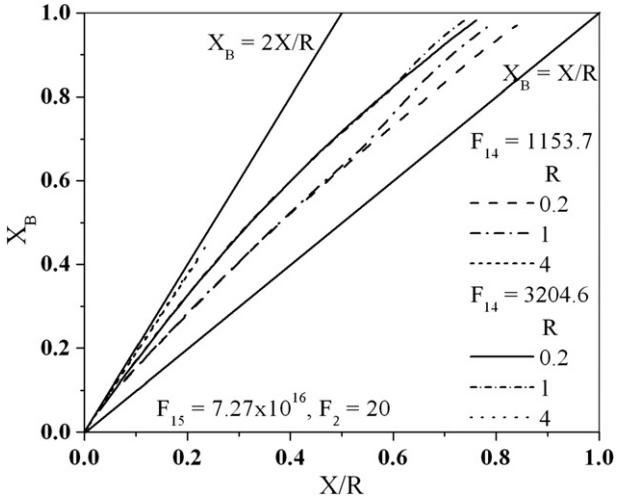

Fig. 5. Relation between X_B and X ($F_3 = 0.005$).

dimensionless groups is as discussed earlier in connection with Fig. 3, the effect of conversion is seen here. While for large R (see the results for $R = 4$), the short chain limit applies over the entire conversion range, for small values of R, it is seen that the oligomers formed at low conversions tend towards short chains, but at larger conversions, the curves remain parallel to the long chain limit, in some cases even moving towards it.

How δ^* depends on conversion may be examined if one assumes the entire polymer formed to contribute to the film thickness as assumed in some earlier models [27,37]. The film thickness at any conversion may be calculated for this case as:

$$\delta_t = \frac{XA_{T0}V_a\alpha_s\left[M_A + \frac{n_x+1}{n_x}M_B\right]}{\rho_p a_{if}} \tag{32}$$

where n_x is the average chain length of the polymer formed till conversion X. Denoting the molecular weight factor in brackets on the right side as M_x, we get, for the non-dimensional thickness as defined in equation (33),

$$\begin{aligned}\delta^* &= X\frac{M_x}{M_{C_0}} \text{ for } R \geq 1 \\ &= \frac{X}{R}\frac{M_x}{M_{C_0}} \text{ for } R \leq 1\end{aligned} \tag{33}$$

The molecular weight ratio appearing in the above equations varies between 1 (for long chains) to 1.59 (for short chains) for the HMDA-HMDI system. In Fig. 6, we show typical results of model simulations for the variation of $\delta^*$with conversion X (or X/R, depending on the value of R in relation to 1). The limiting cases represented by equation (33) for short and long chains are plotted for comparison. Cases where the film thicknesses fall below the lower limiting line are situations in which a significant amount of the polymer formed remains as dissolved in the reaction zone (or as nuclei, although this amount is usually insignificant) over most of the conversion range (mostly for $R \leq 1$and low F_2). In some of these cases, it was necessary to increase the value of n_{max} for satisfactory closure of material balance, and these cases were not studied exhaustively because of the computational intensity of the calculations involved. A comparison between Fig. 6(a) and (b) shows that the short chain limit is relevant only for cases of $R > 1$.

Equation (31), along with the limiting relationships of δ^* and X_B, defines a quadratic in X^*, which may be solved to get an idea of X^* as a function of the system parameters, and hence to conclude whether a given system proceeds under kinetic, diffusion or mixed

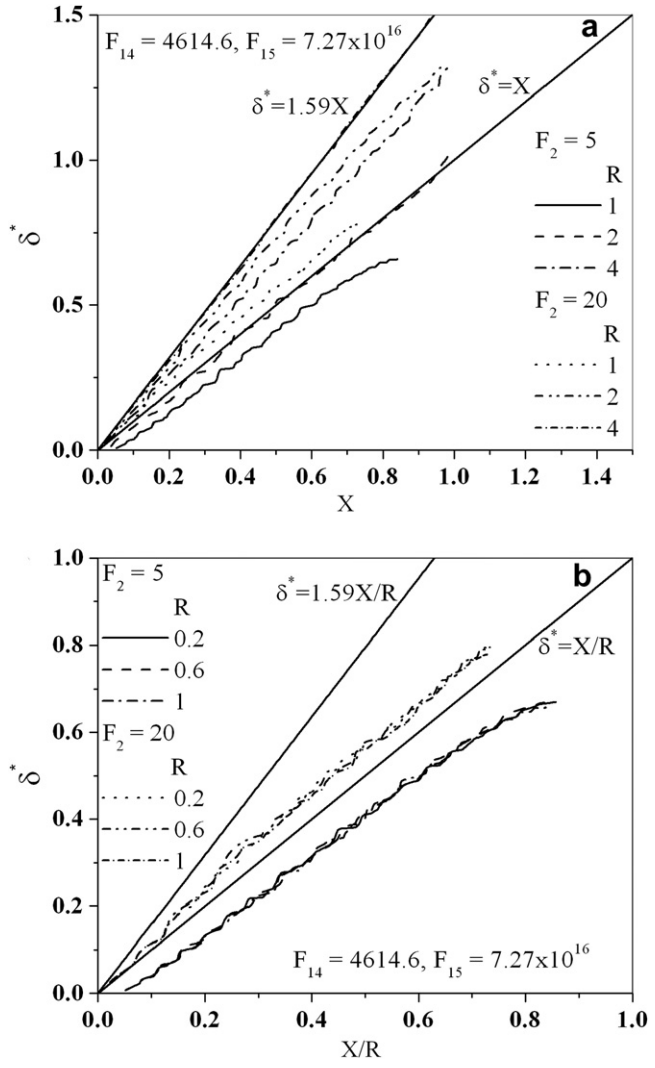

Fig. 6. Relation between δ^* and X for (a) $R \geq 1$ and (b) $R \leq 1$ ($F_3 = 0.005$).

regime. The solution of this resulting quadratic equation for X^* is given below:

$$X^* = \frac{R}{2g}\left[1 \pm \sqrt{1 - \frac{4g}{f}\frac{K_{A0_{sa}}}{F_{14}F_3}}\right] \text{ for } R \leq 1$$
$$= \frac{R}{2g}\left[1 \pm \sqrt{1 - \frac{4g}{f}\frac{K_{A0_{sa}}}{RF_{14}F_3}}\right] \text{ for } R \geq 1 \quad (34)$$

where $f = \frac{M_A + gM_B}{M_A + M_B}$ and $g = \frac{n_x+1}{n_x}$. The short and long chain limits for f are 1.59 and 1, while those for g are 2 and 1 as discussed previously for polyurea system. A necessary condition for a change of regime during a run can immediately be obtained from equation (34) by requiring that the quantity under the square root be positive. This gives, for $R \leq 1$ and assuming the polyurea system,

$$\frac{K_{A0_{sa}}}{F_{14}F_3} \leq 0.25 \text{ or } 0.2, \quad (35)$$

depending on whether the chains are long or short (for $R \geq 1$ the left side of the inequality has to be divided by R). A value of 0.2 may be taken as defining a necessary condition, being the more conservative. Conversely, that the left side is higher than 0.25 is a sufficient condition for no change of regime during a synthesis (the regime remains kinetic throughout). If condition (equation 35) is satisfied, then we can define further conditions under which $0 \leq X^* \leq 1$. An interesting possibility that this analysis shows, which is not intuitively obvious, is that of two physically meaningful roots existing for X^*; under these conditions, the regime shifts from kinetic to diffusion control at an early stage of the reaction, but will revert back to kinetic at a late stage. Physically, this happens because the kinetics can slow down as B gets nearly exhausted, and offer a controlling resistance again. Clearly, these are cases of $R \leq 1$.

Model calculations confirm the above concepts. An illustration is provided in Fig. 7, for a situation in which there is only one regime change (Fig. 7(a)) and one in which there are two (Fig. 7(b)). In these figures, the left side of equation (31) is plotted with conversion, and critical conversions are recognized as those at which this curve intersects the horizontal defined by the right side of equation (31). Equation (34) gives a value of $X^* = 0.31$ for the conditions of Fig. 7(a), which is seen to be close to the actual value predicted by the simulation. For the conditions of Fig. 7(b), there are two roots predicted by equation (34), as 0.0835 and 0.5165, but shown by the simulations to be 0.081 and 0.35 respectively. The discrepancy in the latter value is because the chain length under these conditions is close to neither limit. Such discrepancies are also seen whenever all the polymer is not in the film, as is to be expected.

3.3. Polymer properties

3.3.1. Molecular weight

Fig. 8 shows the development of molecular weight (M_w or M_N, Fig. 8a) and polydispersity (Fig. 8b) with fractional conversion of the limiting monomer. The values of the parameters for Fig. 8 are such that the requirements of kinetic control are satisfied over the entire conversion range. Since the trends for diffusion control are similar, these are not shown. To get an appreciation of the influence of the relative magnitudes of the rate parameters for chain extension and nucleation, F_5 was kept constant and F_4 was varied by over an order of magnitude. Simulations show, as expected, that the effect of varying F_1 in kinetic regime (and conversely, of varying F_4 in diffusion regime) is negligible.

In all cases, the molecular weight starts at low values as expected in step polymerizations. For cases of $R < 1$ (A-monomer in excess), the molecular weight shows a rapid increase towards the end, while it remains low for $R > 1$. This is because the condition in the reaction zone tends towards equimolarity in the former case, as

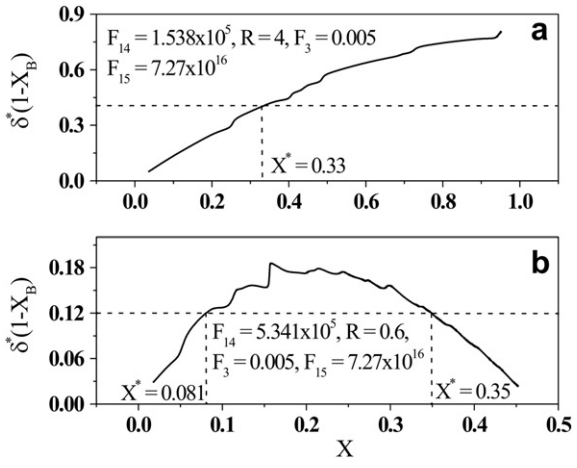

Fig. 7. Prediction of regime shift based on the plot of $\delta^*(1 - X_B)$ vs. X: (a) Conditions which show a single transition from kinetic to diffusion control occur, (b) conditions which show two transitions – from kinetic to diffusion control and back to kinetic control.

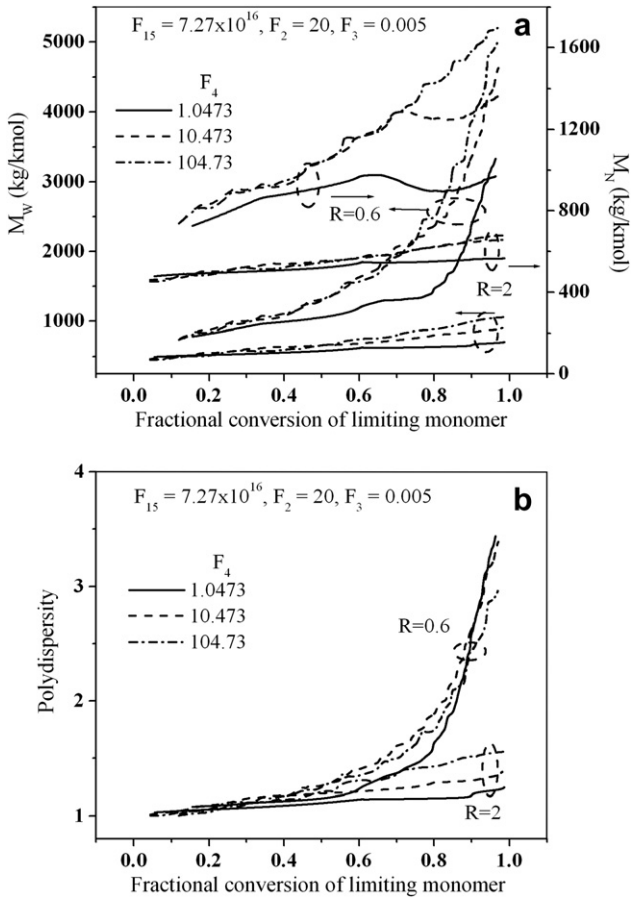

Fig. 8. Development of (a) molecular weights M_w and M_N and (b) polydispersity with conversion in kinetic control: Limiting monomer is *A* if $R > 1$ and *B* if $R < 1$.

the *B*-monomer gets exhausted. If $R > 1$, *B* remains in excess at all times, and prevents the attainment of a high molecular weight. M_N shows much less variation as compared to M_w, showing that the average chain length does not vary a great deal with conversion. This is consistent with the earlier discussion of how various macroscopic parameters (conversion of *B*, film thickness) change with conversion for a given chain length – in most cases, the simulation results would lie close to a line of constant chain length over the entire conversion range. A result of this is that the polydispersity increases more or less similarly to M_w as conversion increases, as Fig. 8(b) shows.

Fig. 8 shows that the larger the value of F_4 for a constantF_5, the larger the molecular weight achieved. This is as expected since F_5 controls the rate at which oligomers are removed from the reaction zone, while F_4 (in kinetic regime) controls the rate at which they grow. Similar would be the effect in diffusion control of F_1. In general, over a large conversion range, the increase in M_w with *X* is more rapid in diffusion regime. This is likely to be because the chain growth in this regime is limited by the rate of supply of *A* to the reaction zone, and the moment a molecule of *A* appears, it is used by two existing *B* type species to form a much longer chain. In kinetic regime by contrast, the molecular weight increases in smaller steps. Because the concentration of *A* in the reaction zone is limited by its partition coefficient, we would expect the above difference in the rate of increase of molecular weight to become more pronounced as the value of *R* decreases, since difference in the concentrations of *A* between kinetic and diffusion regimes increases at small values of *R*. This is illustrated in Fig. 9, in which the molecular weight (M_N) is plotted as a function of conversion, keeping the ratio of the characteristic rates of chain precipitation and chain extension (F_{45} in kinetic regime and F_{15} in diffusion regime) the same in diffusion and kinetic regimes, for $R = 0.6$.

In what follows, we explore the effect of the important dimensionless groups *R*, F_2 and F_{14} on the final molecular weight (Fig. 10a) and polydispersity (Fig. 10b) of the film that is achieved in the reaction. Fig. 10 shows the variation of these properties with the bulk mole ratio *R* for different values of the parameters F_{14} and F_2. Calculation of the trends for different values of F_{15} (keeping F_{14} constant) shows similar trends, and is hence not reported. The values of F_{14} in Fig. 10 are such that the system remains in the kinetic regime throughout (trends in diffusion regime are similar). A monotonically decreasing trend as *R* increases is seen in all cases. Conditions which promote the mole ratio in the reaction zone-to tend towards 1 would be expected to result in a high molecular weight, and the effect of *R* can be understood in that light [3,39]. The nature of the interfacial system is such that concentration equality can never be achieved in the reaction zone, but given this constraint, Table 4 and Fig. 3 show the conditions under which long chains are possible and the stoichiometry of monomer consumption tends towards 1:1. These are conditions of low values of *R*, F_2, F_{14} and F_{15}. This is consistent with the trends seen in Fig. 10.

Fig. 10(b) shows that the polydispersity values decreases towards 1 as *R* increases, showing that conditions which promote low molecular weight also tend to make the MWD narrow. Such a behavior has been experimentally observed recently by Wolinski and Wronski [39]. The polydispersity trends show a peak with *R* in general [39], the peak becoming flatter and ultimately disappearing to give a monotonic decrease as F_2 increases. Fig. 6 shows that at large values of F_2, there is a greater tendency of the curves to follow a constant chain length line more or less over the entire conversion range, and these are clearly conditions that contribute to a low polydispersity. However, the combination of a low polydispersity and a high molecular weight is not impossible, as the curves at small values of *R* and F_2 illustrate.

The effect of the phase volume ratioF_2 in Fig. 10 can be understood through its effect on the monomer concentration and hence the polymerization kinetics. IncreasingF_2 increases the organic phase monomer concentration in the reaction zone and hence increases the concentration inequality in favor of *B* in the reaction zone.

The influence of the competition between the rate processes of chain growth and chain precipitation was earlier commented on in

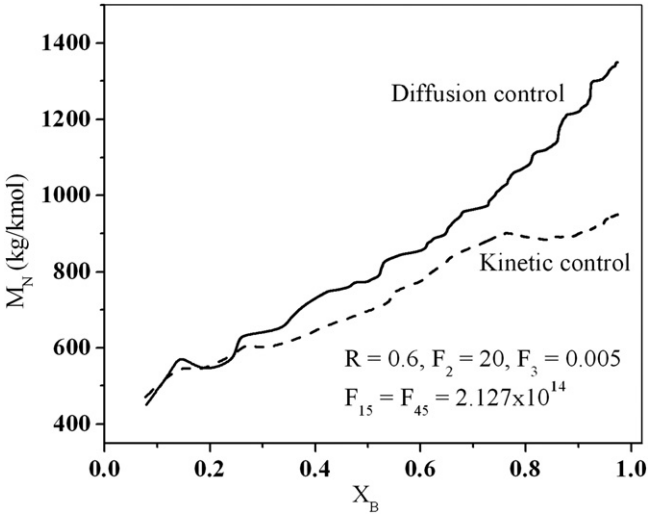

Fig. 9. Comparison of the development of molecular weight M_N with conversion of the limiting monomer in diffusion ($F_{14} = 3.42 \times 10^6$) and kinetic ($F_{14} = 342$) regimes.

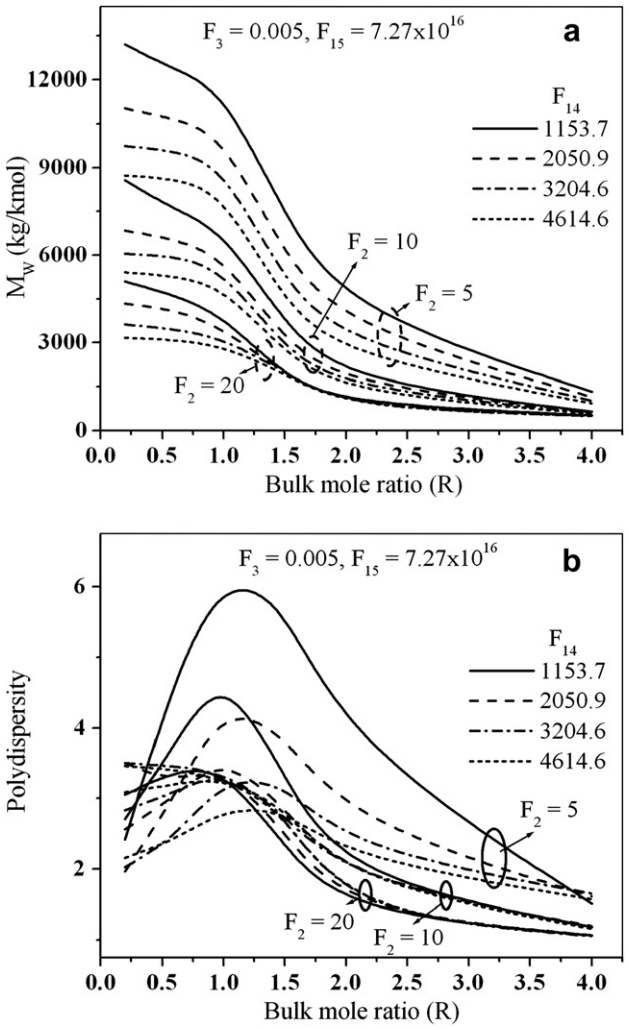

Fig. 10. Final (a) molecular weight M_w and (b) polydispersity of the film vs. R.

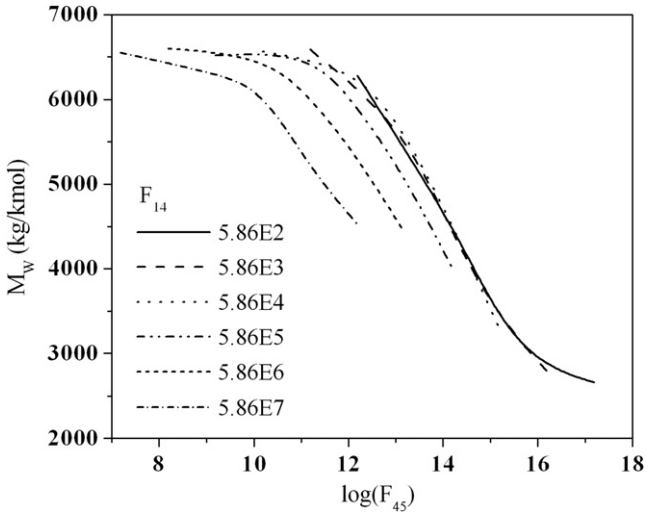

Fig. 11. Final molecular weight of the film vs. F_{45} ($F_3 = 0.005$, $F_2 = 22.22$).

the context of variation of molecular weight during a run. Fig. 11 shows the influence of this competition on the final molecular weight achieved. Here, M_w is plotted as a function of the group F_{45}, which is the ratio of F_5 to F_4. Clearly for small F_{14}, at low values of F_{45} (growth dominating over precipitation), the chain stay and grow in the reaction zone (till presumably they fall out of solution by spinodal decomposition), and one gets a high molecular weight irrespective of the value of the other group shown, F_{14}. As F_{45} increases, the molecular weight decreases, as there is a greater tendency for oligomers to be removed from the reaction zone by precipitation. In this region, the lower the value of F_{14}, the higher the molecular weight achieved, as the system moves well into a kinetically controlled regime. One sees a bunching of curves as F_{14} is increased, since the system moves into diffusion control and the chain growth becomes controlled by diffusion. At larger values of F_{45}, a dominance of nucleation gives low molecular weight.

3.3.2. Crystallinity

Fig. 12 shows the development of crystallinity during the course of IP reaction in kinetic and diffusion control regimes. Qualitatively the trends are similar; the crystallinity either increases monotonically with conversion ($R = 2$), or shows a maximum ($R = 0.6$). For a given set of other parameters and conversion, an increase in F_4 in kinetic regime (or F_1 in diffusion regime) results in a decrease in the crystallinity. We may recall the rapid increase in molecular weight at large conversions for $R \leq 1$. This would result in spinodal decomposition, especially of the longer chains, since these species have a very narrow metastable region. This explains the decreasing trend in crystallinity towards the end.

Just as the molecular weight achieved depends on the competition between the relevant rate process of chain extension and the rate process of precipitation, the crystallinity achieved depends on a competition between the two mechanisms of phase separation, viz, nucleation and growth. Conditions that favor chain growth in the model are precisely conditions that keep the oligomers in solution till the spinodal limit is reached, and hence are conditions that favor a decrease in crystallinity. A correlation between low molecular weight and high crystallinity (and vice versa) may therefore be expected in general. Fig. 13 shows the relationship between molecular weight and crystallinity, and the correlation mentioned above can be seen, as the curve for $R = 1$ and $F_2 = 22.22$ shows. The points on this curve cover a wide range of the groups F_{15} and F_{14}. However, there are other influences since molecular weight also depends significantly on the concentration ratio of the monomers in the reaction zone: for example, we have seen that high values of R lead to low molecular weights, but it is possible for spinodal decomposition to dominate under these conditions and produce a film of low crystallinity. The statement above on the inverse correlation between molecular weight and crystallinity therefore requires to be qualified – it obtains, provided conditions which control the monomer ratio in the reaction zone remain the same. Fig. 13 shows the effect of R and F_2 (which influence, as discussed above, the concentration ratio of monomers in the reaction zone) on the crystallinity-molecular weight correlation, and shows that the curve moves to the left as R increases and as F_2 increases.

3.3.3. Film thickness

Both experimentally and theoretically, film thickness and its variation with time have been important concerns in the literature. Film thickness is clearly an important property in its own right, and experimentally observed dependencies are useful in postulating models. Thus, for example, a square root dependence of thickness on time is taken to imply diffusion control, while a linear dependence signals kinetic control [31,42]. Freger and Srebnik [28] carried out a simulation study and observed that the film thickness-time relationship differs in general from the square root power law in the later stages of the reaction. Experimental results show

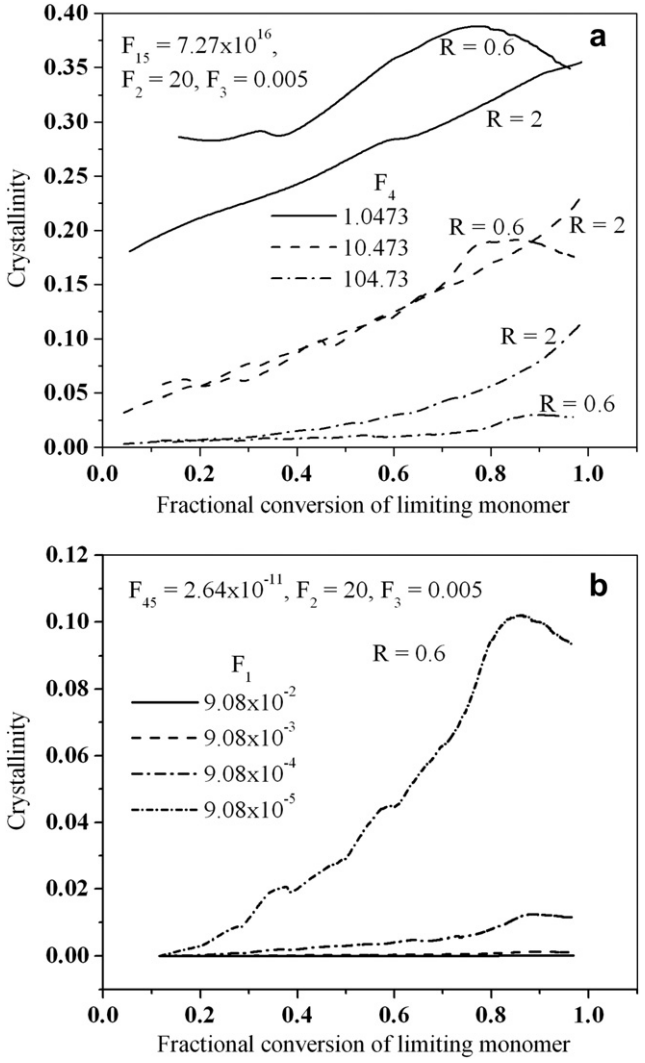

Fig. 12. Crystallinity development in (a) kinetic control and (b) diffusion control: Limiting monomer is *A* if $R > 1$ and *B* if $R < 1$.

considerable variation in the dependence observed, with various values of n in $\delta \propto t^n$ being reported, in the range 0 to 1. Recently, Bouchemal et al. [43] have observed a decrease in n towards the end of reaction. Film formation by IP reaction is a complicated process involving various equilibrium and rate processes. A given synthesis may proceed under kinetic control, or diffusion control, or both, as discussed above. Furthermore, the observed scaling of δ with time even within a regime would depend on whether the polymer formed is mostly in the film or partly in solution. Since the present model considers all the relevant rate and equilibrium processes, we may expect the model to reflect the trends observed in experiments.

Fig. 14 shows, according to the present model, the variation of film thickness with time on logarithmic co-ordinates, under various conditions. Thus, Fig. 14(a) demonstrates the how film thickness scales with time for typical kinetic and mixed regime situations, while Fig. 14(b) shows the same under diffusion control. The slopes reported (i.e., the value of n) are for the best-fit straight lines in the linear region, taken to be the region where the coefficient of regression is greater than 0.99. A value of $n = 1$ is approximated by the kinetic regime runs, at low conversions. For mixed regime, the value lies between 1 and 0.5, while for diffusion regime (Fig. 14(b)), the value is close to 0.5. The tendency for n to decrease at large

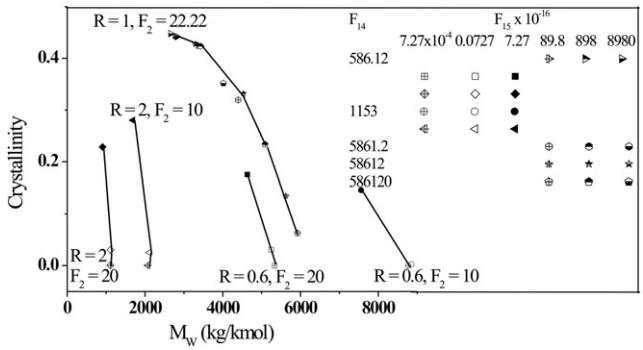

Fig. 13. Inverse correlation between crystallinity and M_w ($F_3 = 0.005$), and effect of parameters which control monomer ratio in the reaction zone on this correlation.

times, as observed by Bouchemal et al. [43] experimentally and Freger and Srebnik [28] in their simulations is seen in all cases. It may also be remarked that the scaling that Bouchemal et al. [43] observe at small times is the square root scaling characteristic of diffusion control. This is as expected by the present model, since their studies are for flat films, for which as remarked earlier, diffusion control is the more likely.

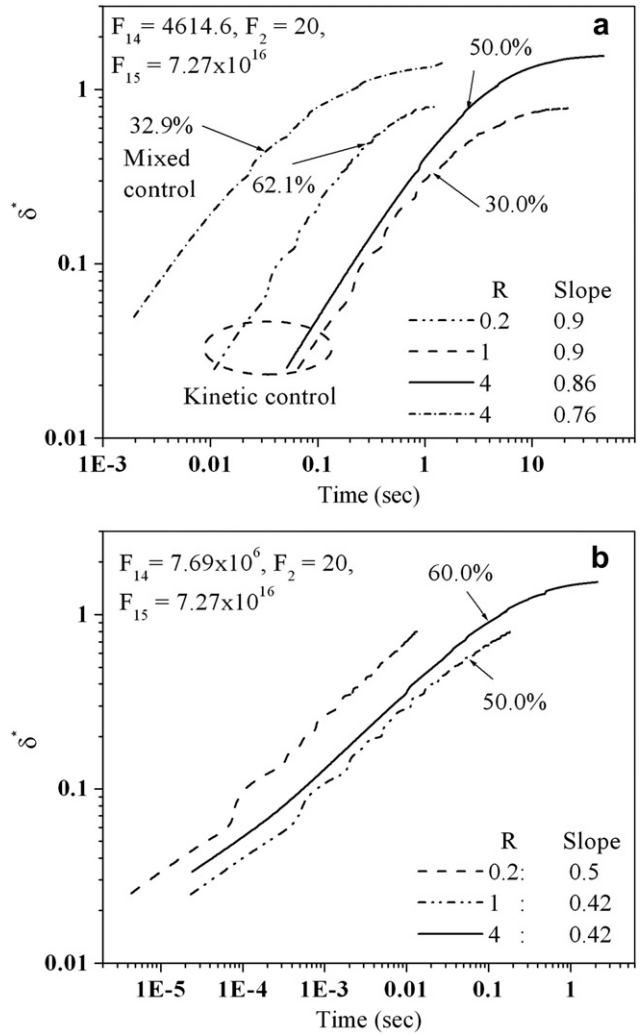

Fig. 14. Film thickness variation with time in (a) kinetic and mixed regimes and (b) diffusion regime. The percentage figures marked on the curves show the conversion of limiting monomer till which the linear region extends.

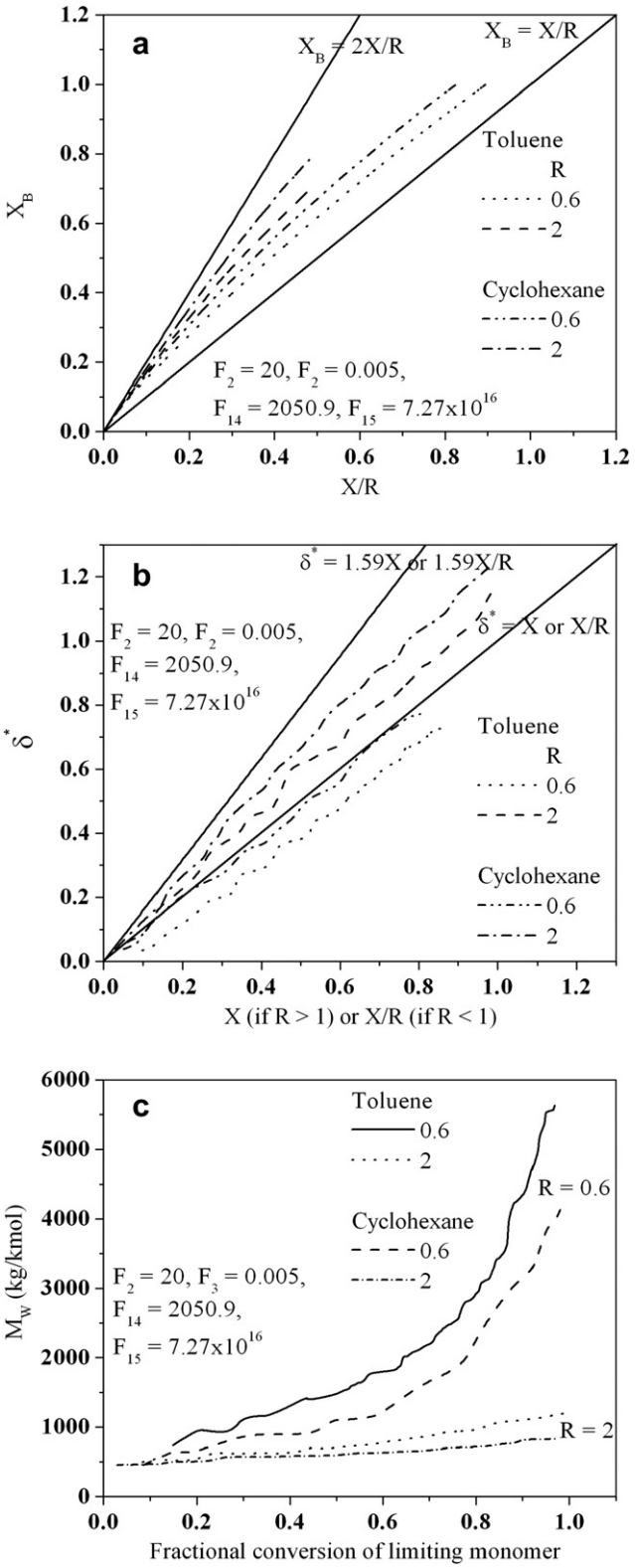

Fig. 15. Solvent effect on (a) X_B vs. X/R (b) δ^* vs. X or X/R and (c) M_w vs. fractional conversion of limiting monomer: Limiting monomer is A if $R > 1$ and B if $R < 1$.

3.3.4. Effect of solvent on film properties

In the discussion thus far, the solvent-related groups have been held constant. The organic solvent used in IP affects the partition coefficient for the aqueous monomer ($K_{A_{0sa}}$), along with the polymer solution thermodynamics [23,34]. Wagh et al. [34] found that

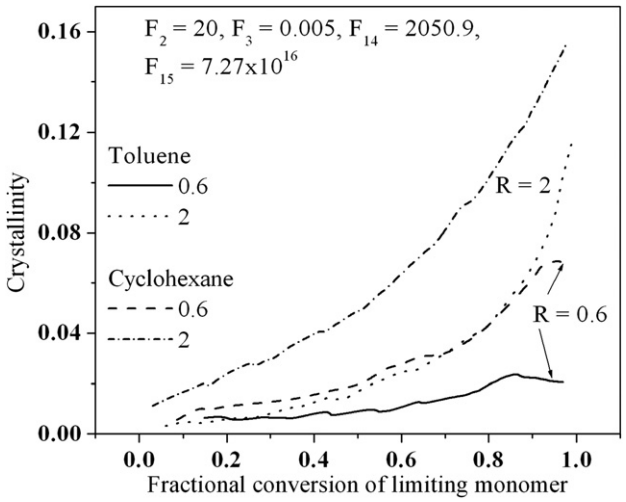

Fig. 16. Solvent effect on crystallinity vs. fractional conversion of limiting monomer: Limiting monomer is A if $R > 1$ and B if $R < 1$.

the effect of solvent on kinetics is more complex than can be explained on the basis of partition coefficient alone. As for polymer properties, existence of a broader metastable region allows the oligomeric species to spend more time and grow to high molecular weights. This behavior is reflected in Fig. 15, which shows a comparison of trends of X_B, δ^* and M_w with conversion, for two solvents, toluene and cyclohexane, chosen here because of the differences in solubility limits (the interaction parametersχ, taking oligomer B_5 as an example, are 2.34 for toluene and 3.31 for cyclohexane). Both Fig. 15(a) and (b) show that the respective variations of X_B and $\delta^*$with conversion are closer to the long chain asymptotes for toluene, the better solvent. A comparison of the curves for $R = 0.6$ in Fig. 15(b) shows that the tendency for the polymer chains to remain in solution in preference to phase-separating out, is higher for toluene. The net result, however, is a higher molecular weight achieved in the case of toluene as Fig. 15(c) demonstrates.

Fig. 16 shows the effect of solvent on the development of crystallinity with conversion for two different values of R. The larger availability of A-monomer in the reaction zone and the broader metastable region in the case of toluene favor chain growth as compared to chain precipitation, and the importance of spinodal decomposition as the mechanism of phase separation increases, relative to nucleation. This results in a low crystallinity.

4. Conclusions

A comprehensive model for interfacial polycondensation has been developed in this work. Broadly, the model shows that the competition between the rate processes of diffusion, reaction and phase separation by nucleation controls most aspects of property development and kinetics in this process, for a given monomer chemistry. Dimensionless groups that capture the relative rates of these phenomena have been identified and their effect on kinetics and film properties explored in some detail. The relative importance of nucleation and spinodal decomposition as two mechanisms of phase separation is what determines the crystallinity of the film in semi-crystalline systems such as polyurea, and this competition is also captured in terms of the same dimensionless groups. In spite of the complexity of the system, an analysis of controlling resistances has lead to the formulation of universal criteria that determine the conditions for kinetic control, diffusion

control and for a change of regime during the reaction. Likewise, the effect of the other important parameters has been shown to lie between limiting cases, which can be derived by analysis. A confirmation of most of the model results is available, in a qualitative or a semi-quantitative sense, in the experimental results reported in the literature. For example, the difference in film properties, for the same polymer, between microencapsulation and unstirred film in a layered system are now seen to be attributable to the difference in regime – the former cases are usually kinetically controlled while the latter are diffusion controlled. While thus a confirmation of the model precepts is available from the literature, more extensive experimentation to confirm specific predictions of the model will be reported shortly.

This work therefore provides a rational basis for the analysis of interfacial polycondensation systems and for designing synthesis conditions to achieve desired results in terms of film properties.

References

[1] LeGrand DG, Bendler JT. Handbook of polycarbonate science and technology. New York: Marcel Dekker; 2000.
[2] Chanda M, Roy SK. Plastic technology handbook. 4th ed. Florida: CRC Press; 2006.
[3] Morgan PW. Condensation polymers: by interfacial and solution methods. New York: Wiley; 1965.
[4] Chang TMS. Science 1964;146(3643):524–5.
[5] Khilar K. A state-of-the-art report on encapsulation. Bombay: IIT; 1987.
[6] Green KD, Gill IS, Khan JA, Vulfson EN. Biotechnology and Bioengineering 1996;49(5):535–43.
[7] Yadav SK, Khilar KC, Suresh AK. Journal of Membrane Science 1997;125(2):213–8.
[8] Torini L, Argillier JF, Zydowicz N. Macromolecules 2005;38(8):3225–36.
[9] Cadotte JE. US Patent 4,039,440, August 2, 1977.
[10] Desai NV, Rangarajan R, Rao AV, Garg DK, Ankleshwaria BV, Mehta MH. Journal of Membrane Science 1992;71(3):201–10.
[11] Peterson RJ. Journal of Membrane Science 1993;83(1):81–150.
[12] Rao AP, Desai NV, Rangarajan R. Journal of Membrane Science 1997;124(2):263–72.
[13] Jeong BH, Hoek EMV, Yan Y, Subramani A, Huang X, Hurwitz G, et al. Journal of Membrane Science 2007;294(1–2):1–7.
[14] Buch PR, Jagan Mohan D, Reddy AVR. Journal of Membrane Science 2008;309(1–2):36–44.
[15] Ghosh AK, Jeong BH, Huang X, Hoek EMV. Journal of Membrane Science 2008;311(1–2):34–45.
[16] Moniruzzaman M, Chattopadhyay J, Billups WE, Winey KI. Nano Letters 2007;7(5):1178–85.
[17] Tarameshlou M, Jafari SH, Khonakdar HA, Farmahini-Farahani M, Ahmadian S. Polymer Composites 2007;28(6):733–8.
[18] Cranmer JH, Tesoro GC, Uhlmann DR. Industrial and Engineering Chemistry Product Research and Development 1982;21(2):185–90.
[19] Salehi-Mobarakeh H, Ait-Kadi A, Brisson J. Polymer Engineering and Science 1996;36(6):778–85.
[20] Hisamoto H, Shimizu Y, Uchiyama K, Tokeshi M, Kikutani Y, Hibara A, et al. Analytical Chemistry 2003;75(2):350–4.
[21] Jong J, Lammertink RG, Wessling M. Lab on a Chip 2006;6(9):1125–39.
[22] Parrish CF. US Patent 7285306, October 23, 2007.
[23] Dhumal SS, Wagh SJ, Suresh AK. Journal of Membrane Science 2008;325:758–71.
[24] Millich F, Carraher Jr CE. Interfacial synthesis. In: Fundamentals, vol. I. New York: Marcel Dekker; 1977.
[25] Millich F, Carraher Jr CE. Interfacial synthesis. In: Polymer Applications and Technology, vol. II. New York: Marcel Dekker; 1977.
[26] Carraher Jr CE, Preston J. Interfacial synthesis. In: Recent Advances, vol. III. New York: Marcel Dekker; 1982.
[27] Yadav SK, Khilar KC, Suresh AK. AIChE Journal 1996;42(9):2616–26.
[28] Freger V, Srebnik S. Journal of Applied Polymer Science 2003;88:1162–9.
[29] Berezkin AV, Khokhlov AR. Journal of polymer science: Part B: Polymer physics 2006;44:2698–724.
[30] Cheng LP, Dwan AH, Gryte CC. Journal of Polymer Science Part B: Polymer Physics 1995;33(2):211–22.
[31] Ji J, Dickson JM, Childs RF, McCarry BF. Macromolecules 2000;33:624–33.
[32] Gonzalez-Ortiz LJ, Asua JM. Macromolecules 1996;29(13):4520–7.
[33] Kamide K, Ijima H, Matsuda S. Polymer Journal 1993;25(11):1113–31.
[34] Wagh SJ, Dhumal SS, Suresh AK. Journal of Membrane Science 2009;328:246–56.
[35] Van Krevelen DW. Properties of polymers—their correlation with chemical structure: their numerical estimation and prediction from additive group contributions. Amsterdam: Elsevier; 1990.
[36] Karode SK, Kulkarni SS, Suresh AK, Mashelkar RA. Chemical Engineering Science 1997;52:3243–55.
[37] Dean JA. Lange's handbook of chemistry. 13th ed. New York: McGraw Hill; 1985.
[38] Yadav SK. Microencapsulation in polyurea shell by interfacial polycondensation. PhD Thesis, Bombay: IIT, 1995.
[39] Wolinski J, Wronski S. Chemical Engineering and Processing: Process Intensification 2009;48(5):1061–71.
[40] Fogler HC. Elements of chemical reaction engineering. 3rd ed. New Delhi: Prentice Hall of India; 1999.
[41] Wagh SJ. Studies in interfacial polycondensation. PhD Thesis, Bombay: IIT, 2004.
[42] Janssen LJJM, Boersma A, Nijenhuis K. Journal of Membrane Science 1993;79:11–26.
[43] Bouchemal K, Couenne F, Briancon S, Fessi H, Tayakout M. AIChE Journal 2006;52:2161–70.